The Astrophysical Journal Letters, 823:L23 (7pp), 2016 June 1 doi:10.3847/2041-8205/823/2/L23

THE SUPERNOVA IMPOSTOR PSN J09132750+7627410 AND ITS PROGENITOR

L. Tartaglia[1,2], N. Elias-Rosa[1], A. Pastorello[1], S. Benetti[1], S. Taubenberger[3,4], E. Cappellaro[1], G. Cortini[5], V. Granata[1,2], E. E. O. Ishida[4,6], A. Morales-Garoffolo[7], U. M. Noebauer[4], P. Ochner[1], L. Tomasella[1], and S. Zaggia[1]
[1] INAF—Osservatorio Astronomico di Padova, Vicolo dell'Osservatorio 5, I-35122 Padova, Italy
[2] Università degli Studi di Padova, Dipartimento di Fisica e Astronomia, Vicolo dell'Osservatorio 2, I-35122 Padova, Italy
[3] European Southern Observatories, Karl-Schwarzschild-Str., D-85748 Garching, Germany
[4] Max-Planck-Institut für Astrophysik, Karl-Schwarzschild-Str. 1, D-85748 Garching, Germany
[5] Osservatorio Astronomico di Monte Maggiore, Predappio, Italy
[6] Clermont Université, Université Blaise Pascal, CNRS/IN2P3, Laboratoire de Physique Corpusculaire, BP 10448, F-63000 Clermont-Ferrand, France
[7] Institut de Ciències de l'Espai (CSIC-IEEC), Campus UAB, Carrer de Can Magrans S/N, E-08193 Cerdanyola del Vallés, Barcelona, Spain
Received 2016 February 21; revised 2016 April 7; accepted 2016 April 14; published 2016 May 23

ABSTRACT

We report the results of our follow-up campaign of the supernova impostor PSN J09132750+7627410, based on optical data covering ∼250 days. From the beginning, the transient shows prominent narrow Balmer lines with P-Cygni profiles, with a blueshifted absorption component becoming more prominent with time. Along the ∼3 months of the spectroscopic monitoring, broad components are never detected in the hydrogen lines, suggesting that these features are produced in slowly expanding material. The transient reaches an absolute magnitude $M_r = -13.60 \pm 0.19$ mag at maximum, a typical luminosity for supernova impostors. Amateur astronomers provided ∼4 years of archival observations of the host galaxy, NGC 2748. The detection of the quiescent progenitor star in archival images obtained with the *Hubble Space Telescope* suggests it to be an 18–20 $M_\odot$ white–yellow supergiant.

Key words: galaxies: individual (NGC 2748) – supernovae: general – supernovae: individual (PSN J09132750+7627410, SN 2007sv, SN 1997bs, SNHunt248)

Supporting material: data behind figure

1. INTRODUCTION

Energetic outbursts of massive stars are often labeled as "supernova impostors" (Van Dyk et al. 2000), since they usually show observational features resembling those of SNe IIn (Schlegel 1990; Filippenko 1997). However, SN impostors are non-terminal outbursts of massive stars, extra-galactic counterparts of the "Great Eruption" (occurred in the 19th century) of the Galactic luminous blue variable (LBV) η-Car. The mechanisms triggering these events are not yet fully understood (Pauldrach & Puls 1990).

In most cases, SN impostors have been related to major outbursts of LBV stars (e.g., Smith et al. 2010; Tartaglia et al. 2015b), since narrow hydrogen lines present in their spectra have inferred expansion velocities comparable to those of LBV winds (10^{2-3} km s^{-1}). LBVs are evolved, luminous (a few 10^{5-6} $L_\odot$) massive stars (>30 $M_\odot$), very close to the Eddington limit, characterized by large instabilities in the outer layers and high mass losses. Nonetheless, LBV-like outbursts have also been linked to lower-mass stars (see, e.g., the case of SN 2008S and other similar transients; Berger et al. 2009; Bond et al. 2009; Botticella et al. 2009; Thompson et al. 2009), while binary interactions can also play an important role in triggering violent mass-loss episodes.

In this context, we report the results of our follow-up campaign of the SN impostor PSN J09132750+7627410 (hereafter PSNJ09+76). Its discovery was announced on 2015 February 10 through an IAU Central Bureau Astronomical Telegram[8] in NGC 2748, which previously hosted two other SNe: the Type Ia SN 1985A (Wild & Schildknecht 1985; Wegner & McMahan 1987) and the Type Ic SN 2013ff (Brimacombe et al. 2013). PSNJ09+76 was classified as an SN impostor by Tartaglia et al. (2015a) on 2015 February 12.

Hereafter, we will adopt a luminosity distance of $D_L = 23.8 \pm 2.0$ Mpc, hence a distance modulus of $\mu = 31.88 \pm 0.18$ mag, as reported by the Extragalactic Distance Database[9] (Tully et al. 2009). For the foreground Galactic extinction, we will assume $A(V) = 0.073$ mag (Schlafly & Finkbeiner 2011). We adopted no host galaxy contribution to the total extinction, since in the spectra of PSNJ09+76 there is no evidence of the narrow Na ID absorption feature at the recessional velocity of NGC 2748.

2. OBSERVATIONS AND DATA REDUCTION

The follow-up campaign of PSNJ09+76 was carried out using the 1.82 m Copernico telescope equipped with AFOSC located at Mount Ekar, Asiago, Italy; the 10.4 m Gran Telescopio Canarias (GTC) with OSIRIS; and the 2.56 m Nordic Optical Telescope (NOT) with ALFOSC, both located at the Observatorio del Roque de los Muchachos, La Palma, Spain. Additional photometric data, mostly covering the pre-eruptive phases, were provided by public archives and amateur astronomers. The transient was also observed by the UV/Optical Telescope (UVOT) on board the *Swift* Gamma-ray Observatory.[10] UVOT data (*uvw2, uvm2, uvw1, U, B, V* bands) were processed using the HEASARC software (HEASoft[11], version 6.17) following the prescription of Poole et al. (2008). The transient field was also observed by the *Hubble Space*

[8] http://www.cbat.eps.harvard.edu/unconf/followups/J09132750+7627410.html
[9] http://edd.ifa.hawaii.edu/
[10] http://swift.gsfc.nasa.gov/
[11] http://heasarc.nasa.gov/lheasoft/

Telescope (*HST*) in the optical domain and the *Spitzer Space Telescope* (*SST*) in near-infrared (NIR), and we used these images to perform our analysis on the progenitor of PSNJ09 +76 (see Section 5).

Ground-based spectroscopic and photometric data were pre-processed in the usual manner (overscan, bias, and flat-field corrections) using standard IRAF[12] tasks. The magnitudes of the transient were measured through a dedicated pipeline (SNOoPY; Cappellaro 2014) and calibrated with reference to a set of field stars. This local sequence was calibrated with reference to Sloan Digital Sky Survey (SDSS[13]) fields obtained during photometric nights, while their *BVRI* magnitudes were derived from the Sloan magnitudes following the relations in Chonis & Gaskell (2008). Unfiltered data from the amateur astronomers were calibrated to the *r*-band.

The spectroscopic calibrations were performed using spectra of standard stars obtained during the same nights (for the flux calibration) and spectra of comparison lamps obtained with the same instrumental setup used (for the wavelength calibration). The wavelength calibration was checked using night sky lines, shifting the spectra in case of discrepancy. The flux calibration was checked using the magnitudes obtained on the closest nights, and a scaling factor was applied when necessary. Finally, we corrected the spectra of PSNJ09+76 for the Galactic foreground extinction and for the redshift ($z = 0.0049$) due to the recessional heliocentric velocity of the host galaxy ($1476 \pm 2\,\mathrm{km\,s^{-1}}$).

3. PHOTOMETRIC ANALYSIS

The outcomes of our photometric measurements are shown in Figure 1, while the magnitudes in the different bands are reported in the online table.

Our *i*-band image obtained on 2015 May 25 with ALFOSC (the one with the best seeing among our photometric data, full width at half maximum: FWHM $\sim 0\farcs5$) was used to accurately pinpoint the position of the transient (R.A. = 09:13:27.408, decl. = +76:27:40.91; J2000).

About four years of archival data were provided mostly by amateur astronomers and revealed no further eruptive episodes similar to that observed in 2015. The last non-detection prior to the 2015 event is dated 2015 January 6, ∼1 month before our first *r*-band point. The *r*-band maximum occurred on 2015 February 16 (MJD = 57069.76), and we consider this as the reference epoch for the phases.

After maximum, we note a relatively fast decline in the *u*-band light curve with a slope of 6.8 mag/100 days. The light curves decline more slowly in the other bands, with 4.3 mag/100 days, 2.8 mag/100 days, and 3.3 mag/100 days in the *B*-, *V*-, and *g*-bands, respectively. The *r*-band light curve shows a decline rate of 1.9 mag/100 days in the first ∼130 days, while it steepens at later epochs. A similar behavior is observed in the *i*- and *z*-band light curves, with 1.3 mag/100 days and 0.4 mag/100 days in the first ∼100 days, while the slopes increase to 5.2 mag/100 days and 4.8 mag/100 days, respectively, at later phases.

The evolution of the $B - V$ and $r - i$ colors is shown in Figure 1(b). We note that the colors become progressively redder, consistent with a rapid decline of the temperature of the emitting gas. The color evolution at early phases is similar to those of other impostors (Figure 1), although we note that PSNJ09+76 is much redder than the other transients at phases later than ∼50 days from maximum.

The *r*-band absolute light curve is shown in panel (c). Assuming the distance modulus and the extinction reported in Section 1, we infer an *r*-band absolute peak magnitude of -13.60 ± 0.19 mag, corresponding to a pseudo-bolometric luminosity $\gtrsim 10^{41}\,\mathrm{erg\,s^{-1}}$ (panel (d)). The comparison with the absolute light curves of similar transients shows that PSNJ09 +76 has an absolute light curve similar to those of other SN impostors, with the main outburst having a light curve resembling those of a core-collapse SN, but with a fainter peak magnitude.

4. SPECTROSCOPIC ANALYSIS

The results of the spectroscopic analysis are shown in Figure 2. In panel (a), we show the final sequence of spectra obtained during the ∼3 months of our spectroscopic follow-up campaign. A log of the spectroscopic observations is reported in Table 1, along with the information on the instrumental setup used, exposure times, and spectral resolutions.

The spectra at early phases are characterized by a blue continuum with sharp and narrow Balmer lines with P-Cygni profiles, as also noticed by Humphreys & Gordon (2015). The temperature of the pseudo-continuum, estimated through a blackbody fit, rapidly falls from $13{,}400 \pm 2500$ K to 3400 ± 400 K, in agreement with the estimated broadband color evolution (Figure 1(b)). The Hα profile is characterized by a prominent P-Cygni profile at all phases.

In Figure 2(b), we show the detailed evolution of the Hα and Hβ regions. The total Hα profile is well fitted using a Gaussian component in absorption and a single Lorentzian component in emission. From this fit, at early phases, we derive an FWHM velocity $<700\,\mathrm{km\,s^{-1}}$ for the emission component and a nearly constant (900–$1000\,\mathrm{km\,s^{-1}}$) expansion velocity, deduced from the positions of the minimum of the absorption components. Nonetheless, at +39 days and +92 days, we note a second absorption component (Figure 2(b)), suggesting the presence of a slower shell, moving at 300–$450\,\mathrm{km\,s^{-1}}$, which is nearly the same value (within the errors) inferred from the FWHM of the narrow emission component at the same phases. The absence of this component at earlier phases, as well as in other spectra at similar phases, is most likely due to insufficient resolution. The velocity inferred from the blue wing of the faster absorption components in the +39 day spectrum is consistent with that of the red wing of the Hα emission profile. We do not detect the same features in the Hβ profile, although this might be related to the lower signal-to-noise ratio (S/N) of our spectra at the corresponding wavelengths.

The Hγ line is also identified at early phases. In our +39 day spectrum, we also identify Fe II (multiplets 27, 37, 38, 42, 48, 49), Ba II $\lambda\lambda$4554.0, 4934.1, Na ID $\lambda\lambda$5889.9, 5895.9, O I at 7774 Å and Ca II(H and K), Ti II (multiplets 1, 19, 20, 31, 34, 41, 51, 82, 105), and, tentatively, the Ba I (multiplet 2). We note that our last (+92 day) spectrum has a much redder continuum, and broad features appear, most likely due to TiO molecular bands in the 6100–6400 Å and 7000–7400 Å regions.

[12] http://iraf.noao.edu/
[13] http://sdss.org

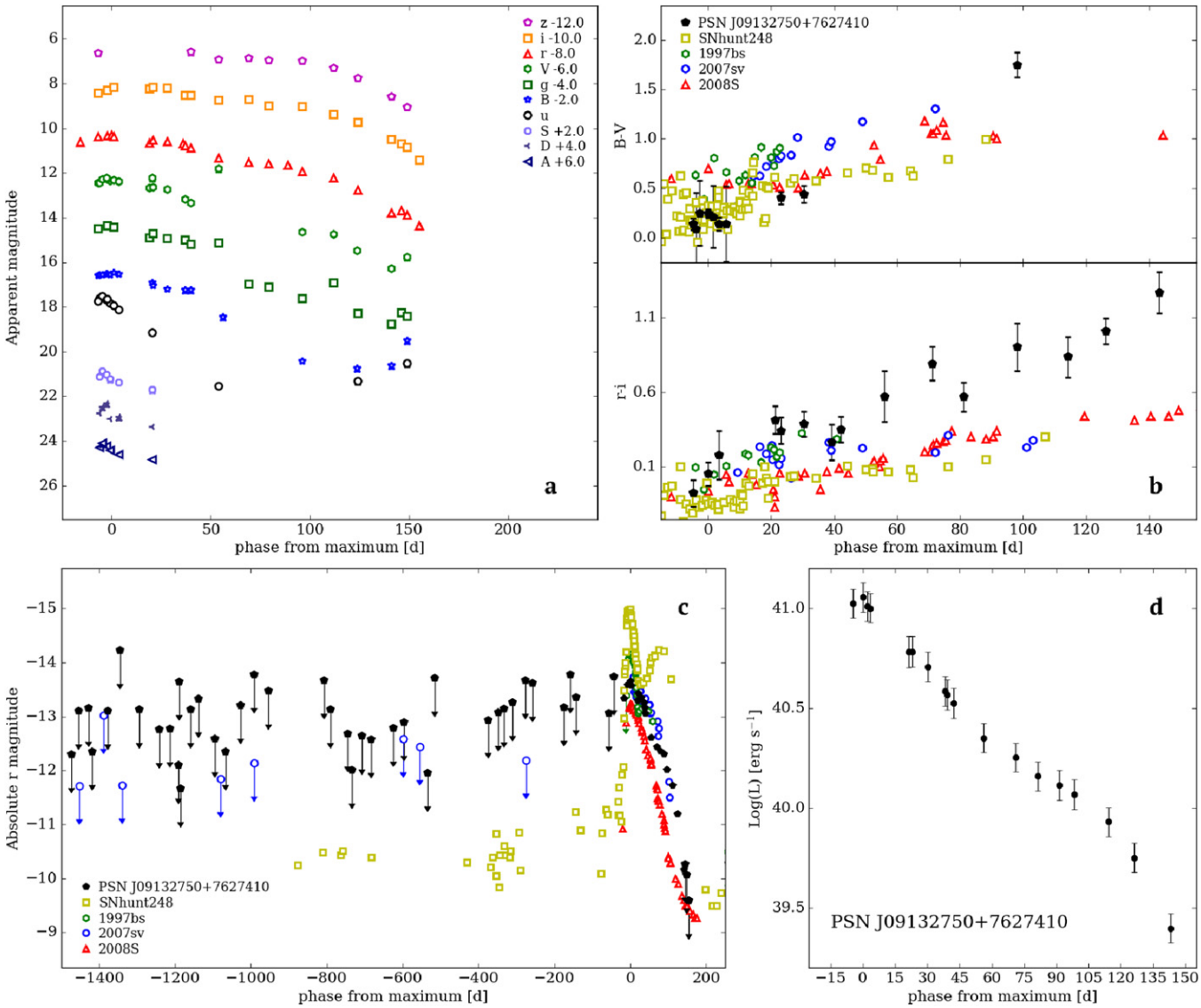

Figure 1. (a) Multi-band light curves of PSNJ09+76. Arbitrary constants were added to the different magnitudes. (b) $B - V$ and $r - i$ color evolutions of PSNJ09 +76, compared to those of other SN impostor data (2007sv, 1997bs, and the peculiar transient 2008S, whose nature is still debated; see, e.g., Prieto et al. 2008; Botticella et al. 2009; Pumo et al. 2009; Smith et al. 2009; Thompson et al. 2009; Wesson et al. 2010; Kochanek 2011; Szczygiełet al. 2012; Adams et al. 2015). Distance moduli and reddening estimates of 1997bs ($\mu = 31.1$ mag, $A_V = 0.093$ mag), 2007sv ($\mu = 31.38$ mag, $A_V = 0.056$ mag), SNhunt248 ($\mu = 31.76$ mag, $A_V = 0.140$ mag), and 2008S ($\mu = 28.74$ mag, $A_V = 1.13$ mag) were taken from Van Dyk et al. (2000), Tartaglia et al. (2015b), Kankare et al. (2015), and Botticella et al. (2009), respectively. (c) Historical absolute r-band magnitudes of PSNJ09+76 compared to those of a sample of different transients. r- and i-band magnitudes for 2007sv, 1997bs, 2008S, and SNhunt248 were obtained from the R- and I-band magnitudes adding the constants 0.16 mag and 0.37 mag, respectively, following the transformations given by Blanton & Roweis (2007). (d) Pseudo-bolometric light curve of PSNJ09+76 computed integrating the observed fluxes from the UV to the optical domains. The luminosity is obtained integrating the computed SED with the trapezoidal rule (see Section 3.4 of Tomasella et al. 2013 for more details) The magnitudes used for this figure are reported in the data file.

(Data used to create panel (a) of this figure are available.)

5. THE PROGENITOR STAR OF PSNJ09+76

Deep archival *HST* images[14] of the host galaxy were obtained on 2001 July 6 (*HST* ID proposal: 9042; PI: S. Smartt) using the Wide Field Planetary Camera 2 (WFPC2) with the *F*450*W* and *F*814*W* filters. Also, three sets of mid-infrared (MIR) *SST* images were obtained on 2009 December 2, 2010 April 12 (ID proposal: 61063; PI: K. Sheth), and 2014 January 2 (ID proposal: 10046; PI: D. Sanders) using the Infra-Red Array Camera (IRAC) with the 3.6 and 4.5 μm channels (channels 1 and 2, respectively). These data were retrieved from by the *Spitzer* Heritage Archive[15](SHA), hence fully co-added and calibrated. Drizzled *HST* images (resampled to a uniform grid to correct geometric distortions, with $\sim$0.1 arcsec pixel^{-1}) obtained through the *Hubble* Legacy Archive[16](HLA) and Post Basic Calibrated Data (pbcd) *SST* images (with $\sim$0.6 arcsec pixel^{-1}), were aligned to our i-band ALFOSC image (with 0.19 arcsec pixel^{-1}) obtained on 2015

[14] http://archive.stsci.edu/hst/search.php

[15] http://sha.ipac.caltech.edu/applications/Spitzer/SHA/

[16] http://hla.stsci.edu/

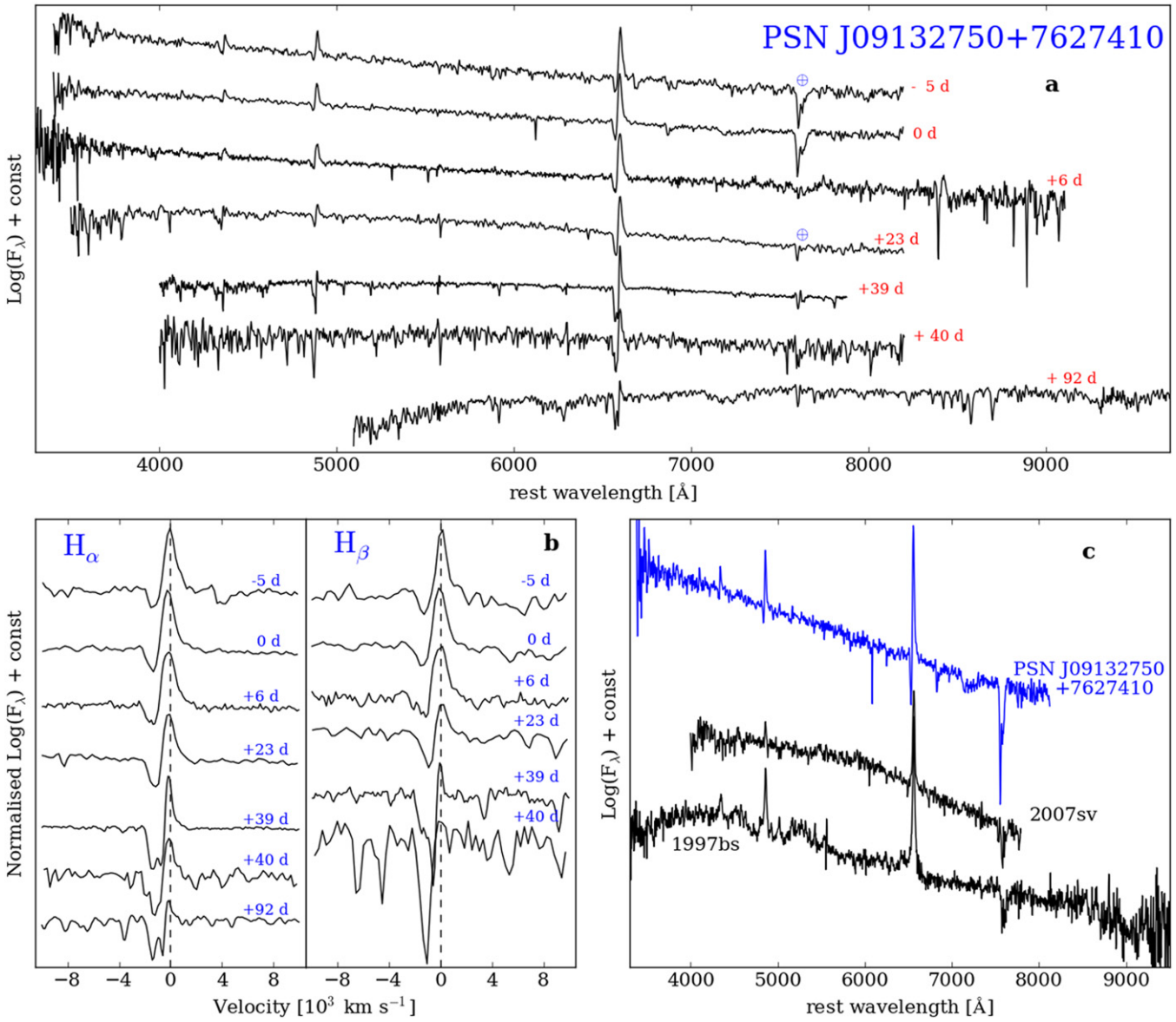

Figure 2. (a) Spectral sequence of PSNJ09+76. The phases are reported to the right and are referred to the *r*-band maximum. ⊕ symbols mark the positions of the strongest telluric absorption bands. (b) Evolution of the Hα (left) and Hβ (right) line profiles in velocity space. Vertical dashed lines mark the rest-wavelength position of the two lines. (c) Comparison between the spectra of PSNJ09+76 obtained at the epoch of the *r*-band maximum and those of the SN impostors 2007sv and 1997bs at similar phases. All spectra have been dereddened and redshift corrected, and shifted by an arbitrary constant.

Table 1
Log of the Spectroscopic Observations of PSNJ09+76

Date	Phase	Instrumental Setup	Grism or Grating	Spectral Range (Å)	Resolution (Å)	Exp. Times (s)
2015 Feb 12	−5	Ekar182+AFOSC	2xgm4	3400–8200	14.4	2 × 1800
2015 Feb 16	0	Ekar182+AFOSC	gm4	3400–8200	14.4	2700
2015 Feb 23	6	NOT+ALFOSC	gm4	3500–9000	18.1	2400
2015 Mar 11	23	Ekar182+AFOSC	gm4	3400–8200	14.4	2 × 2700
2015 Mar 26	38	GTC+OSIRIS	R1000B	3600–8000	7.0	2 × 1800
2015 Mar 28	40	Ekar182+AFOSC	gm4	3400–8200	14.4	2 × 2700
2015 May 18	92	GTC+OSIRIS	R1000R	5000–10000	8.0	2 × 1800

Note.
The phases are relative to the maximum.

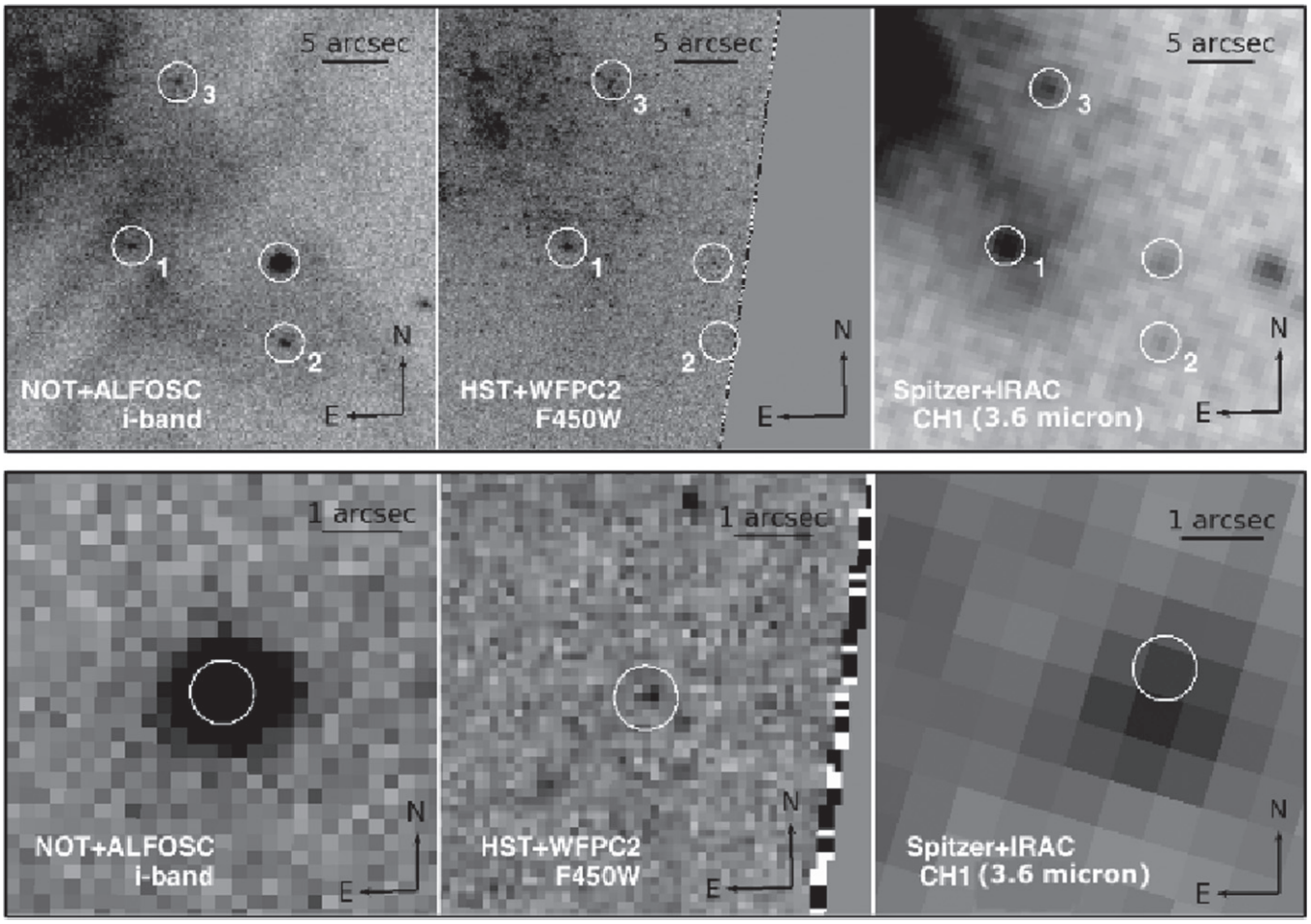

Figure 3. Pre-eruption archival images of the site of PSNJ09+76. Top: details of the ALFOSC *i*-band image obtained on 2015 May 25, the *HST* $F450W$ image and the *SST* image obtained on 2010 April 12. The positions of three reference stars are also shown. Bottom: zoom-in of the position coincident with that of PSNJ09+76 in the ALFOSC images. The positions in the *HST* and *SST* images are those computed using the GEOMAP and GEOXYTRAN IRAF tasks.

May 8. Geometrical alignments were performed using the IRAF task GEOMAP and a maximum of 17 common point-like sources between all sets of images. The errors of the geometric transformations are the rms uncertainties given by GEOMAP, obtaining a precision in the corresponding position of PSNJ09 +76 of $<0\farcs020$.[17]

We identify a source at the position of the transient (within the transformation errors) in both *HST* and *SST* images, although, given the different spatial resolution, the source in the *SST* images is most likely the blend of multiple sources (see Figure 3). *HST* magnitudes and errors of the source in the VEGAMAG flight system ($F450W = 24.27 \pm 0.17$ and $F814W = 24.00 \pm 0.18$ mag) were obtained using the DOLPHOT package[18] (Dolphin 2000). The DOPLHOT output provides also a set of parameters that can be used to interpret the nature of the different sources. The detected source has an "object-type" flag of "1," which means that it is likely stellar. Accounting for the extinction ($A_{F450W} = 0.093$ mag, $A_{F814W} = 0.044$ mag) and distance modulus reported before, we estimate for the progenitor candidate the absolute magnitudes of -7.71 ± 0.25 mag and -7.95 ± 0.25 mag for filters $F450W$ and $F814W$, respectively.

The source magnitudes in the *SST* images were measured using the SPOT[19] package, integrating the flux in a 4×4 pixel area around the position of the progenitor, which included the whole extended source seen in Figure 3 (bottom right panel). We obtained 3.1×10^{-19} and 1.7×10^{-19}, 3.0×10^{-19} and 0.8×10^{-19}, 2.7×10^{-19} and 1.4×10^{-19} erg s^{-1} cm^{-2} Å^{-1}, resulting in the approximate magnitudes of 18.3 and 18.0 mag, 18.3 and 18.8 mag, 18.5 and 18.2 mag in channels 1 and 2 from the images obtained with *SST* on 2009 December 2, 2010 April 12, and 2014 January 2, respectively. As we can see, there is no clear evidence of an excess of emission (e.g., due to dust formation) between 2009 and 2014 at 3.6 μm, but some variability is perceptible at 4.5 μm. However, we note that the resulting magnitudes are likely due to the contribution of multiple sources in the vicinity of the progenitor.

[17] We obtained the following transformation uncertainties: $(x, y) = 0\farcs013$, $0\farcs018$ (11 stars used) and $(x, y) = 0\farcs019$, $0\farcs020$ (15 stars used) in the $F450W$ and $F814W$ images, respectively, $(x, y)_1 = 0.066$, $0\farcs072$ (16 stars), $(x, y)_2 = 0.047$, $0\farcs084$ (16 stars), $(x, y)_1 = 0.078$, $0\farcs060$ (17 stars), $(x, y)_2 = 0.066$, $0\farcs072$ (16 stars), and $(x, y)_1 = 0.028$, $0\farcs034$ (12 stars), $(x, y)_2 = 0.072$, $0\farcs090$ (15 stars) for the channel 1 and 2 of images obtained with *SST* on 2009 December 2, 2010 April 12, and 2014 January 2, respectively.

[18] http://americano.dolphinsim.com/dolphot/. We used the WFPC2 Module, v.2.0 (updated in 2014 November).

[19] http://ssc.spitzer.caltech.edu/warmmission/propkit/spot/

6. DISCUSSION AND CONCLUSIONS

In this Letter, we have discussed the outcomes of our photometric and spectroscopic monitoring of the optical transient PSNJ09+76. Its *r*-band absolute magnitude at peak ($M_r = -13.60 \pm 0.19$ mag) is consistent with that expected during giant eruptions of massive stars. In Figures 1(b) and (c), we have shown that the light curves of these transients may differ in terms of absolute magnitudes and color evolutions.

At all phases, the spectra of PSNJ09+76 are characterized by prominent Balmer lines showing sharp and narrow P-Cygni profiles. In our +39 day and +92 day best-resolution spectra, we notice two components in absorption in the Hα profile. Multiple absorptions were also reported in a moderate-resolution spectrum of PSNJ09+76 obtained by Humphreys & Gordon (2015) around maximum. The clear detection of two absorption components suggests the presence of two expanding shells moving at different velocities (namely, $\sim$1000 km s^{-1} and $\sim$340–450 km s^{-1}). The velocity inferred for the slower component is comparable with the FWHM velocity of the narrow emission component visible in both +39 day and +92 day spectra. This shell, initially photo-ionized, quickly recombines and contributes to a large fraction of the narrow Hα flux. The higher-velocity component is likely due to the presence of a further shell, moving at a higher velocity. The absence (or weakness) of the emission component is indicative that this shell is likely outer. Despite the lack of any evidence of shell–shell collision from our data of PSNJ09+76, we speculate that one of the shells may have been expelled in past outbursts.

The analysis of deep pre-outburst archival images obtained with *HST* and *SST* revealed the presence of a source at the position of PSNJ09+76 (within the errors of our relative astrometry). In order to better constrain the nature of the candidate progenitor, we estimated the oxygen abundance at the position of the source following Hakobyan et al. (2009) and the prescriptions of Tremonti et al. (2004) and Pilyugin et al. (2004; see also Pastorello et al. 2015 for more details), which resulted in $12 + \log[O/H] \simeq 8.59$ dex. This value is very close to the solar abundance, 8.69 ± 0.05 dex (Asplund et al. 2009). However, following Smartt et al. (2009), who sets $12 + \log[O/H] = 8.4$ dex as the dividing line between solar and subsolar metallicity evolutionary tracks, we conclude that the environment of PSNJ09+76 is likely at solar metallicity.

The comparison of the observed photometry with ATLAS synthetic spectra[20] (Castelli & Kurucz 2004) suggests an effective temperature of the quiescent progenitor of $\sim$7250 K (Figure 4), resulting in a luminosity of $\mathrm{Log}(L/L_\odot) \simeq 5$ (with a bolometric correction derived from the synthetic spectrum of -0.012 mag). These values of color and luminosity of the recovered precursor candidate suggest a progenitor mass in the range $18-20\,M_\odot$ (see Figure 4). Thus, the progenitor candidate of PSNJ09+76 is likely a moderate-mass white–yellow supergiant, possibly an A-F-type star.

Similar results were also obtained by Kankare et al. (2015) and Smith et al. (2010), who found moderate-mass progenitors ($M \lesssim 20\,M_\odot$) for SNhunt248 and UGC 2773-OT, respectively. The implication from these observational constraints is that not only extremely massive stars can experience large outbursts and hence produce SN impostors.

[20] http://www.stsci.edu/hst/observatory/crds/castelli_kurucz_atlas.html

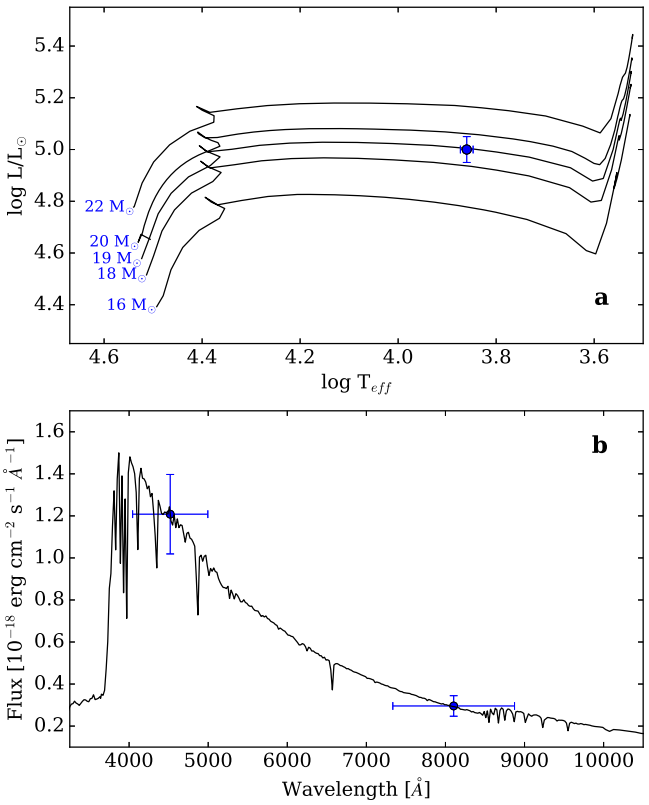

Figure 4. (a) Hertzsprung–Russel diagram showing the position of the PSNJ09+76 progenitor candidate (blue circle). Evolutionary tracks (from 16 $M_\odot$ to 23 $M_\odot$) computed using the Cambridge STARS (Eldridge & Tout 2004) models are also shown. The tracks were obtained assuming solar metallicity. (b) Observed SED of the candidate progenitor (blue circles, with uncertainties). An ATLAS synthetic spectrum for a star with $T_{\rm eff} = 7250$ K, $\log(g) = 1.5$, and solar metallicity is also plotted.

We thank G. Cortini (Monte Maggiore Observatory, Predappio, Italy), F. Martinelli and R. Mancini for their observations obtained on 2011 April 2 and 2013 September 2, respectively. S.T. and U.M.N. acknowledge support by TRR33 "The Dark Universe" of the German Research Foundation (DFG). L.T., N.E.R., A.P., and S.B. are partially supported by PRIN-INAF 2014 (project "Transient universe: unveiling new types of stellar explosions with PESSTO"). Based on observations made with: The Cima Ekar 1.82 m Telescopio Copernico of the Istituto Nazionale di Astrofisica of Padova, Italy. The Gran Telescopio Canarias (GTC) operated on the island of La Palma at the Spanish Observatorio del Roque de los Muchachos of the Instituto de Astrofisica de Canarias. The Nordic Optical Telescope (NOT), operated by the NOT Scientific Association at the Spanish Observatorio del Roque de los Muchachos of the Instituto de Astrofisica de Canarias. Based in part on data collected at Okayama Astrophysical Observatory and obtained from the Subaru Mitaka Okayama Kiso Archive (SMOKA), operated by the Astronomy Data Center, National Astronomical Observatory of Japan. Based in part on observations made with the NASA/ESA *Hubble Space Telescope*, obtained from the Hubble Legacy Archive, which is a collaboration between the Space Telescope Science Institute (STScI/NASA), the Space Telescope European Coordinating Facility (ST-ECF/ESA) and the Canadian Astronomy Data Centre (CADC/NRC/CSA). This work is based in part on observations made with the *Spitzer Space Telescope*, operated

by the Jet Propulsion Laboratory, California Institute of Technology under a contract with NASA. The Swift analysis software is part of HEASoft (the High Energy Astrophysics Software), which encompasses FTools and XANADU (i.e., XSPEC, XRONOS and XIMAGE for spectral, timing and image analysis respectively). IRAF is distributed by the National Optical Astronomy Observatory, which is operated by the Associated Universities for Research in Astronomy, Inc., under cooperative agreement with the National Science Foundation. DOLPHOT is a stellar photometry package adapted from HSTPHOT for general use.

REFERENCES

Adams, S. M., Kochanek, C. S., Prieto, J. L., et al. 2015, MNRAS, submitted (arXiv:1511.07393)
Asplund, M., Grevesse, N., Sauval, A. J., & Scott, P. 2009, ARA&A, 47, 481
Berger, E., Soderberg, A. M., Chevalier, R. A., et al. 2009, ApJ, 699, 1850
Blanton, M. R., & Roweis, S. 2007, AJ, 133, 734
Bond, H. E., Bedin, L. R., Bonanos, A. Z., et al. 2009, ApJL, 695, L154
Botticella, M. T., Pastorello, A., Smartt, S. J., et al. 2009, MNRAS, 398, 1041
Brimacombe, J., Zaggia, S., Barbieri, M., et al. 2013, CBET, 3647, 1
Cappellaro, E. 2014, SNOoPy: a package for SN photometry, http://sngroup.oapd.inaf.it/snoopy.html
Castelli, F., & Kurucz, R. L. 2004, arXiv:astro-ph/0405087
Chonis, T. S., & Gaskell, C. M. 2008, AJ, 135, 264
Dolphin, A. E. 2000, PASP, 112, 1383
Eldridge, J. J., & Tout, C. A. 2004, MNRAS, 353, 87
Filippenko, A. V. 1997, ARA&A, 35, 309
Groh, J. H., Hillier, D. J., Damineli, A., et al. 2009, ApJ, 698, 1698
Hakobyan, A. A., Mamon, G. A., Petrosian, A. R., Kunth, D., & Turatto, M. 2009, A&A, 508, 1259
Humphreys, R. M., Davidson, K., Jones, T. J., et al. 2012, ApJ, 760, 93
Humphreys, R. M., & Gordon, M. S. 2015, ATel, 7172, 1
Kankare, E., Kotak, R., Pastorello, A., et al. 2015, A&A, 581, L4
Kochanek, C. S. 2011, ApJ, 741, 37
Kurucz, R. 1993, ATLAS9 Stellar Atmosphere Programs and 2 km s^{-1} grid. Kurucz CD-ROM No. 13 (Cambridge, MA: Smithsonian Astrophysical Observatory), 18
Makarov, D., Prugniel, P., Terekhova, N., Courtois, H., & Vauglin, I. 2014, A&A, 570, A13
Pastorello, A., Hadjiyska, E., Rabinowitz, D., et al. 2015, MNRAS, 449, 1954
Pauldrach, A. W. A., & Puls, J. 1990, A&A, 237, 409
Pilyugin, L. S., Vílchez, J. M., & Contini, T. 2004, A&A, 425, 849
Poole, T. S., Breeveld, A. A., Page, M. J., et al. 2008, MNRAS, 383, 627
Prieto, J. L., Kistler, M. D., Thompson, T. A., et al. 2008, ApJL, 681, L9
Pumo, M. L., Turatto, M., Botticella, M. T., et al. 2009, ApJL, 705, L138
Schlafly, E. F., & Finkbeiner, D. P. 2011, ApJ, 737, 103
Schlegel, E. M. 1990, MNRAS, 244, 269
Smartt, S. J., Eldridge, J. J., Crockett, R. M., & Maund, J. R. 2009, MNRAS, 395, 1409
Smith, N., Ganeshalingam, M., Chornock, R., et al. 2009, ApJL, 697, L49
Smith, N., Li, W., Silverman, J. M., Ganeshalingam, M., & Filippenko, A. V. 2011, MNRAS, 415, 773
Smith, N., Miller, A., Li, W., et al. 2010, AJ, 139, 1451
Smith, N., Vink, J. S., & de Koter, A. 2004, ApJ, 615, 475
Szczygieł, D. M., Prieto, J. L., Kochanek, C. S., et al. 2012, ApJ, 750, 77
Tartaglia, L., Pastorello, A., Benetti, S., et al. 2015a, ATel, 7051, 1
Tartaglia, L., Pastorello, A., Taubenberger, S., et al. 2015b, MNRAS, 447, 117
Thompson, T. A., Prieto, J. L., Stanek, K. Z., et al. 2009, ApJ, 705, 1364
Tomasella, L., Cappellaro, E., Fraser, M., et al. 2013, MNRAS, 434, 1636
Tremonti, C. A., Heckman, T. M., Kauffmann, G., et al. 2004, ApJ, 613, 898
Tully, R. B., Rizzi, L., Shaya, E. J., et al. 2009, AJ, 138, 323
Van Dyk, S. D., Peng, C. Y., King, J. Y., et al. 2000, PASP, 112, 1532
Wegner, G., & McMahan, R. K. 1987, AJ, 93, 287
Wesson, R., Barlow, M. J., Ercolano, B., et al. 2010, MNRAS, 403, 474
Wild, P., & Schildknecht, T. 1985, IAUC, 4031, 3